SPAWAR
Systems Center
San Diego

TECHNICAL REPORT 1797
June 1999

Measurement of Low-Altitude Infrared Transmission

C. R. Zeisse
SSC San Diego

B. D. Nener
University of Western Australia

R. V. Dewees
NAVAIRWARCEN, China Lake

SSC San Diego

TECHNICAL REPORT 1797
June 1999

Measurement of Low-Altitude Infrared Transmission

C. R. Zeisse
SSC San Diego

B. D. Nener
University of Western Australia

R. V. Dewees
NAVAIRWARCEN, China Lake

SPAWAR
Systems Center
San Diego

SSC San Diego
San Diego, CA 92152–5001

SSC SAN DIEGO
San Diego, California 92152–5001

H. A. Williams, CAPT, USN
Commanding Officer

R. C. Kolb
Executive Director

ADMINISTRATIVE INFORMATION

The work described in this report was performed for the Office of Naval Research (ONR 322) by the Tropospheric Branch, Code D833, SSC San Diego.

Released by
W. L. Patterson, Acting Head
Tropospheric Branch

Under authority of
R. A. Paulus, Acting Head
Propagation Division

ACKNOWLEDGMENTS

Dr. Scott Sandgathe and Dr. Ronald Rerek of the United States Office of Naval Research supported this work. Mr. Arie de Jong of the TNO Physics and Electronics Laboratory, the Netherlands, supplied the long path transmission data shown in the inset of figures 6 and 7 of this report.

EXECUTIVE SUMMARY

OBJECTIVE

Review how the atmosphere influences infrared transmission. Describe a transmissometer suitable for low-altitude measurements of transmission and scintillation in the infrared window regions.

RESULTS

The optical properties of molecules and aerosol particles and the optical phenomena of refraction and interference are the primary factors influencing infrared transmission. A transmissometer was used to measure longwave and midwave infrared transmission and scintillation within several meters of the surface of San Diego Bay. The transmissometer has a black body source, a midwave detector made from InSb, and a longwave detector made from HgCdTe. The instrument achieves an accuracy of ±10% when measuring transmission at a range of 7 km, has a maximum useful transmission range of 18 km in the longwave and 90 km in the midwave, and has a maximum useful scintillation range of 20 km in the midwave.

CONTENTS

Figures

Tables

1. INTRODUCTION

Infrared propagation at low altitudes is a more complex phenomenon than it is at higher altitudes in the troposphere and stratosphere. The following effects influence infrared propagation along low-altitude horizontal paths: (1) molecular extinction, (2) aerosol extinction, (3) refraction (including focusing, defocusing, and mirage formation), and (4) interference. Since each of these four effects is ultimately a manifestation of the meteorological state of the atmosphere, infrared transmission is subject to all the randomness, variability, and unpredictability associated with the weather.

This report reviews the influence of these mechanisms on infrared transmission at low altitudes and then describes the design, operation, and limitations of a transmissometer suitable for measuring broadband atmospheric transmission and scintillation in coastal regions. The instrument operates at infrared wave numbers in two of the infrared atmospheric windows, namely, the midwave band at 3 to 5 μm (2000 to 3333 cm^{-1}) and the longwave band at 8 to 12 μm (833 to 1250 cm^{-1}). The transmissometer is designed to investigate the relationship between aerosols and refraction and measurable meteorological parameters such as wind speed and direction, sea and air temperature, and relative humidity.

Absolute measurements of transmission are desirable for the development and validation of atmospheric transmission models. This report describes a method to calibrate the transmissometer that does not depend on the properties of any of the optical surfaces in the instrument, nor on the responsivity of the detectors.

2. HOW THE ATMOSPHERE INFLUENCES INFRARED TRANSMISSION AND SCINTILLATION

This review of atmospheric phenomena emphasizes effects that influence transmission measurement and transmissometer design. Our starting point will be free-space transmission. Free-space transmission, generally thought of as "100% transmission," is the transmission that would be observed at full range in free space where there are no molecules, no aerosols, and all rays are straight. In a real atmosphere, molecules and aerosols absorb and scatter radiation, reducing the transmission below its free-space value. In addition, atmospheric gases will increase the optical index a few hundred parts per million above the free space value of unity. Such changes in the index may introduce refractive effects such as focusing and defocusing. As a result, transmission measured in a real atmosphere is usually less than the free-space value but may occasionally exceed it in clear air when refractive focusing occurs.

2.1 EXTINCTION BY MOLECULES

Inside the infrared transmission windows where our instrument operates, molecular extinction (absorption and scattering) is controlled primarily by the number of water molecules in the air (i.e., by the absolute humidity), secondarily by the temperature, and only minimally by the pressure. Figure 1 shows how the molecular (clear air) transmission varies with absolute humidity in the midwave and longwave infrared bands.

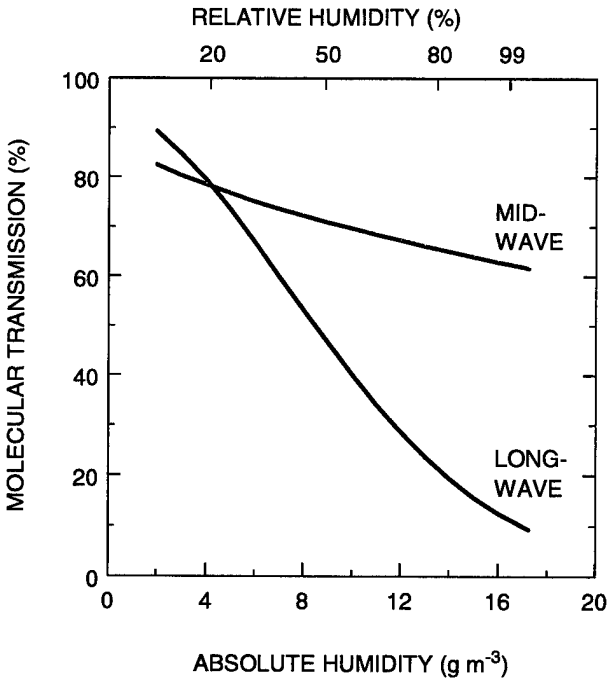

Figure 1. Broadband molecular transmission as a function of absolute humidity. These curves are predicted by MODTRAN 3.5 for propagation through a 1976 Standard Atmosphere. The air temperature is 20°C and the range is 7 km. The relative spectral responsivity for each band is given in figures 10 (longwave band) and 11 (midwave band).

These curves have been calculated with MODTRAN (Berk, Bernstein, and Robertson, 1989; Kneizys et al., 1988) for a 1976 standard atmosphere, an air temperature of 20°C, and a range of 7 km. They give the average wide-band molecular transmission, τ_m, according to the formula:

$$\tau_m\{r(\nu)\} = \frac{\int \tau_m(\nu) r(\nu) d\nu}{\int r(\nu) d\nu}. \quad (1)$$

Here, ν is the wave number and $r(\nu)$ is the relative spectral responsivity of the observation equipment. For the particular calculation shown in figure 1, we have used the relative spectral responsivities for our instrument (figures 10 and 11).

Over the open ocean, the relative humidity is typically 80% so the midwave transmission over the ocean would be about 65% at 7 km whereas the longwave transmission would be less, about 20%. Furthermore, the midwave band is less sensitive to water vapor than the longwave band, as shown by the different slopes of these two lines. If, for example, the relative humidity were to vary between 50 and 90% on a particular day, longwave transmission would vary by 35% but the midwave transmission would vary by only 8%. The single reliable feature of our transmission data has been this one: a relatively constant midwave molecular transmission.

The dependence of molecular transmission on range is shown in figure 2 for a relative humidity of 80% (an absolute humidity of 14.0 g m^{-3}). The longwave transmission is strongly attenuated compared to the midwave transmission. Each of the curves in figure 2 is almost, but not quite, a straight line. In other words, the molecular transmission of a broadband system does not decay exponentially with range. Beer's Law (McClatchey et al., 1978) is strictly obeyed only by laser systems, which operate at a single wave number. Systems (such as the instrument described here), which operate over a range of wave numbers, do not obey Beer's Law. The rich molecular line structure that reflects the strong, rapid variation of molecular absorption coefficient from one wave number to the next explains the difference. A spectral average amounts to a sum over exponentials which, in this case, differ greatly from one another. Such a sum is not itself an exponential.

2.2 EXTINCTION BY AEROSOL PARTICLES

Aerosol extinction can easily dominate the transmission along 10-km paths, especially in the midwave band where molecular transmission is generally high. Aerosol particles over the open ocean usually consist of primary particles from sea spray, consisting of water drops containing various amounts of dissolved salt, or secondary particles such as sulfate arising from the oxidation of dimethyl sulfide. The saltwater particles are approximately spherical with radii ranging very roughly from 0.1 to 10 μm, and they are made when the wind breaks up the ocean surface. The larger, heavier drops are found close to (within several meters of) the ocean surface and, if the wind were suddenly to cease, would rapidly leave the air by dropping into the ocean. The smaller, lighter drops are found at altitudes of several tens of meters and tend to float in the air for hours or days even without much wind.

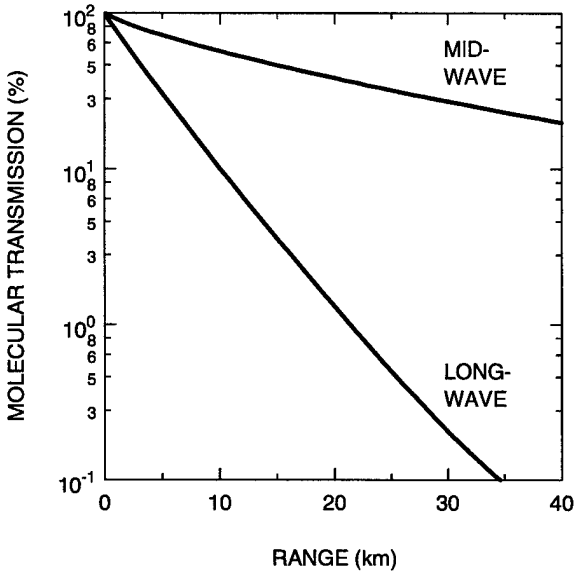

Figure 2. Molecular transmission as a function of range. The absolute humidity is 14 g $\cdot m^{-3}$ (a relative humidity of 80%). Other conditions are the same as for figure 1.

Given the particle size distribution, $dN(r)$, defined as the number of particles per unit volume with radii between r and $r + dr$, the optical extinction produced by particles of all radii can be predicted (McCartney, 1976) by Mie theory from the formula:

$$\sigma_p(\nu) = \int_0^\infty \pi r^2 Q_{ext}(\nu, r, \tilde{n}) \frac{dN}{dr} dr. \qquad (2)$$

Here, Q_{ext} is the efficiency factor given by Mie theory as a function of wave number, particle radius, and complex optical index, $\tilde{n}$. The Mie efficiency factor is the dimensionless ratio of the optical cross section for extinction to the physical cross section, πr^2, of the particle. The Mie extinction coefficients, $\sigma_p(\nu)$, vary much more gradually from one wave number to the next than the molecular extinction coefficients.

In coastal areas, additional complications arise. Man-made pollutants, dense coastal fog, or heavy surf may be present and, if so, they will seriously invalidate the common assumption (which we also make) that conditions are homogeneous along the entire path. However, we *are* fortunate with respect to aerosol particles in that, for the broad bands we encounter with our instrument, Beer's Law remains a good approximation caused by the smooth variation of aerosol extinction coefficient, $\sigma_p(\nu)$, with wave number. Hence, for aerosol transmission at range, L, we may write

$$\tau_p(\nu) = \exp\{-\sigma_p(\nu) L\}. \qquad (3)$$

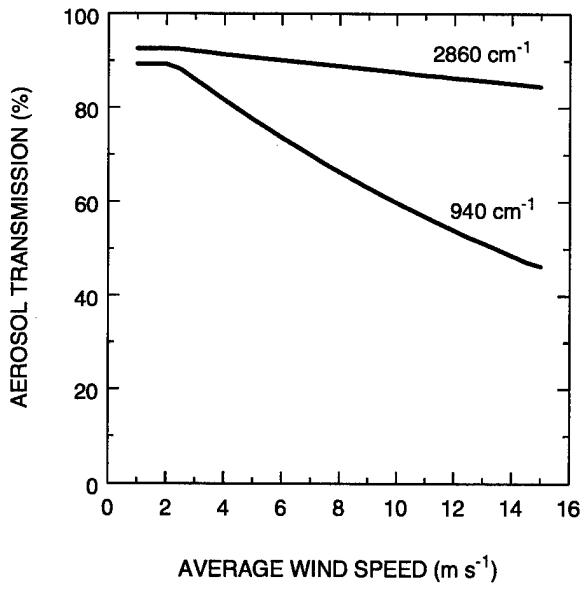

Figure 3. Monochromatic aerosol transmission as a function of average 24-hour wind speed. The curves are labeled with wave number of the optical radiation. The range is 7 km. Each curve was derived from a particle size distribution given by the Navy aerosol model using Mie theory [equation (2)] and Beer's Law [equation (3)].

Much current aerosol research concentrates on determining the particle size distribution and its dependence on meteorological parameters such as wind speed, wind direction, and fetch. Once the distribution is modeled or measured, the optical properties of the polydispersion can be calculated with equations (2) and (3), and as long as the particles are spherical with a well-behaved optical index, this calculation is regarded as routine. As an example of aerosol transmission and its meterological dependence, we show in figure 3 the predictions which follow from the Navy Aerosol Model (Gathman, 1983) for the size distribution of aerosol particles found close to the surface of the open ocean. In this model the size distribution depends empirically on the following four parameters: (1) the air mass parameter, (2) the average wind speed during the previous 24 hours, (3) the current wind speed, and (4) the relative humidity. Figure 3 has been drawn for an air mass parameter of 10, a current wind speed of 10 m s^{-1}, and a relative humidity of 80%. For small values of the average wind speed during the previous 24 hours, the wind has just increased to 10 m s^{-1} and there are few particles in the aerosol of size comparable to the optical wavelength, λ. Hence, the extinction is small and the transmission is high. For large values of the average wind speed over the previous 24 hours, aerosol particles of a size comparable to the optical wavelength have previously been produced and they scatter the light, increase the extinction, and reduce the transmission.

2.3 REFRACTION

In contrast to free space where optical rays are straight, optical rays within the atmosphere can bend towards or away from the earth depending on the atmospheric refractive index gradient. For infrared wave numbers, the refractive index (Hill, Clifford, and Lawrence, 1980; Andreas, 1988) of air depends on temperature, pressure, and humidity. For the moment, we wish to consider only those variations in the refractive index that are gradual in time (change slower than a 10-minute period) and space (change over distances of many tens of meters).

A consequence of a gradually changing refractive index is a continual variation of the angle at which infrared radiation is received (Lawrence and Strohbehn, 1976). There will generally be a vertical temperature gradient in the air above the sea and that gradient will often show a slow variation throughout the day. The temperature gradient will produce, in turn, an index gradient. The rays passing through the index gradient will be bent by an amount depending on its value. Hence, the bending will show a daily variation if the air temperature shows a daily variation. The bending will

change the angle of arrival of the rays but not their intensity. Figure 4 shows the amount of bending expected on the basis of Monin-Obukhov similarity theory (Liu, Katsaros, and Businger, 1979) for a 7-km path when the transmitter and the receiver are both at an altitude of 3 m. The inputs to this model are the air–sea temperature difference, shown on the abscissa in figure 4, and the wind speed, shown as a parameter in the figure. We have used a linear atmosphere for this calculation, meaning that the modified optical refractivity, M, varies linearly with altitude, h. With this crude assumption, and with equal receive and transmit heights, the receive angle and the launch angle are both equal and each is given by the simple expression,

$$\alpha = -\frac{L}{2}\frac{dM}{dh}. \qquad (4)$$

Here, L is the range in km and dM/dh is the (assumed constant) gradient of modified optical refractivity in M-units per m.

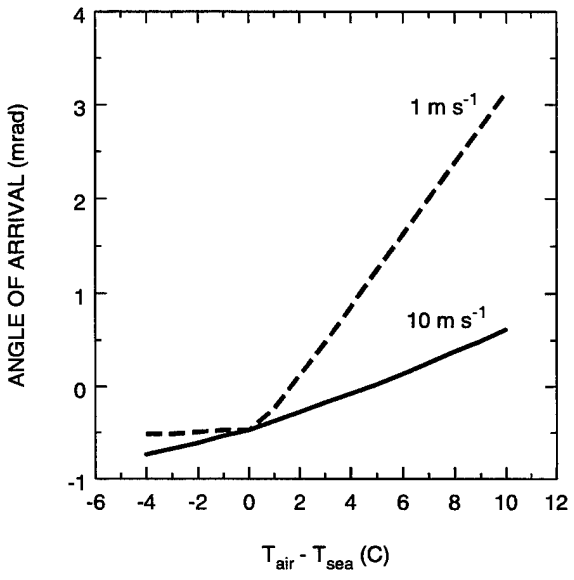

Figure 4. Variation of arrival angle of a ray that has traversed a 7-km path through the atmosphere. The air-sea temperature difference is given on the abscissa. An angle of 0 mrad corresponds to a ray parallel to the earth at (on the local horizon of) the receiver.

As figure 4 shows, for wind speeds varying up to 10 m s^{-1} and air–sea temperature differences varying by several degrees Centigrade about zero, the variation in angle of arrival amounts to several mrad. This variation may cause difficulties if the field of view of the receiver was unable to accommodate this change. As an example, figure 5 shows the complete loss of midwave signal, between times 311.65 and 311.72, along a low-altitude, 7-km path. These data were taken with separate receivers for each band. In each receiver, a detector 1 mm in diameter was mounted at the focus of a primary mirror whose focal length was 1.2 m. A beam initially propagating parallel to the optical axis of the receiver would produce a spot centered on the detector. That spot would reach the edge of the detector in this system if the arrival angle of the entering beam changed by 0.4 mrad. During this experiment, we often experienced a gradual loss of the signal and usually found that readjusting the receiver mount would restore the signal. Figure 5 shows an example of such an event. During the time period figure 5 shows, the mount was not readjusted for either receiver, but the air–sea temperature difference rose from about -2°C to about +2°C and the wind speed increased from about 1 to 6 m s^{-1}. Given these changes and the values in figure 4, it seems likely that on this occasion the spot wandered off the midwave detector and then back on again.

Solutions to this problem (and their drawbacks) may include the use of: (1) a larger detector (that has more noise), (2) a faster primary mirror (that is more expensive), and (3) a field lens (complicating the optics and also adding expense). The field-lens solution will be discussed in subsequent paragraphs.

In addition to this variable bending, which occurs very generally at all elevations, certain refractive effects become noticeable for elevations very close to the ocean surface where significant temperature gradients occur, and for relatively long paths greater than about 10 km. These effects, although rarer than molecular or aerosol effects, can be observed under special circumstances. These circumstances include the situation in which neighboring rays may be brought closer together than their free-space counterparts (the rays are focused), or in which the opposite is true (the rays are defocused). Reflections and mirages may also occur. These effects cause comparatively radical redirection of the ray bundles, leading to their capture when they would be lost under more ordinary conditions.

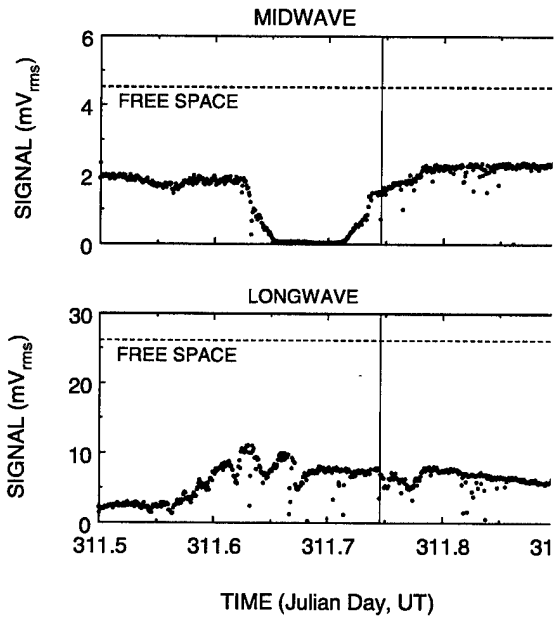

Figure 5. Minute-by-minute data for transmission on a 7-km path over San Diego Bay. There is a separate receiver for each band. These data span a 9.6-hour time interval during day 311 of November 1966. Ships blocking the low-altitude beam probably cause isolated low-transmission values that occur simultaneously in each band (for example, at the vertical time mark near 311.75). The deep minimum in the midwave band (between times 311.65 and 311.72) is probably caused by refractive wander in the midwave receiver. Signals are voltages at the lock-in. (Note: The detectors for these data are *not* the detectors described in the rest of this report.)

Figures 6 and 7 show how refractive effects such as horizon visibility and mirage formation may influence an infrared signal received at low altitude. Figure 6 is a ray trace, presented on a flat-earth diagram, for propagation through an atmosphere specified by the modified optical refractivity based on the meteorological conditions that occurred at a particular time, day 319.7708 of 1996, along a 15-km path above San Diego Bay. In the figure, rays are launched from the transmitter towards the receiver with an angular spread of 3.5 mrad (full angle). Rays launched towards the ocean surface appear to be reflected from the surface, but they are not. Instead, they are bent upward by a strong refractivity gradient in the air just above the surface; they are *mirage* rays. In figure 6, no rays reach the receiver; the receiver is below the horizon. We would expect no signal to be observed. The actual transmission measured at this time was 1/20 of the free-space value, or 5%. (This small positive signal value is easily explained by "leakage" into the receiver aperture, something that would be evident if a more realistic coverage diagram replaced this ray trace.) In figure 7, 2 hours later, the ray trace is similar but the tide has fallen by a fraction of a meter, putting the receiver not only above the horizon, but also into a mirage. In figure 7, rays reach the receiver in two ways, either directly (by passing through a 2-m altitude near mid-path) or as a mirage (by passing through a several centimeter altitude near mid-path). The actual transmission measured at this time was 1.93 times the free-space value, or 193%. These examples show that (1) refractive phenomena may exert a strong influence on

low-altitude infrared propagation, and (2) refractive effects that reduce the signal are indistinguishable from conventional extinction mechanisms brought about by molecules and aerosols.

We represent all large-scale, long-time refractive effects by the propagation factor, F, which is defined (Freehafer et al., 1951) as the ratio of the electric field received in a transparent refractive medium to the electric field that would be received in free space.

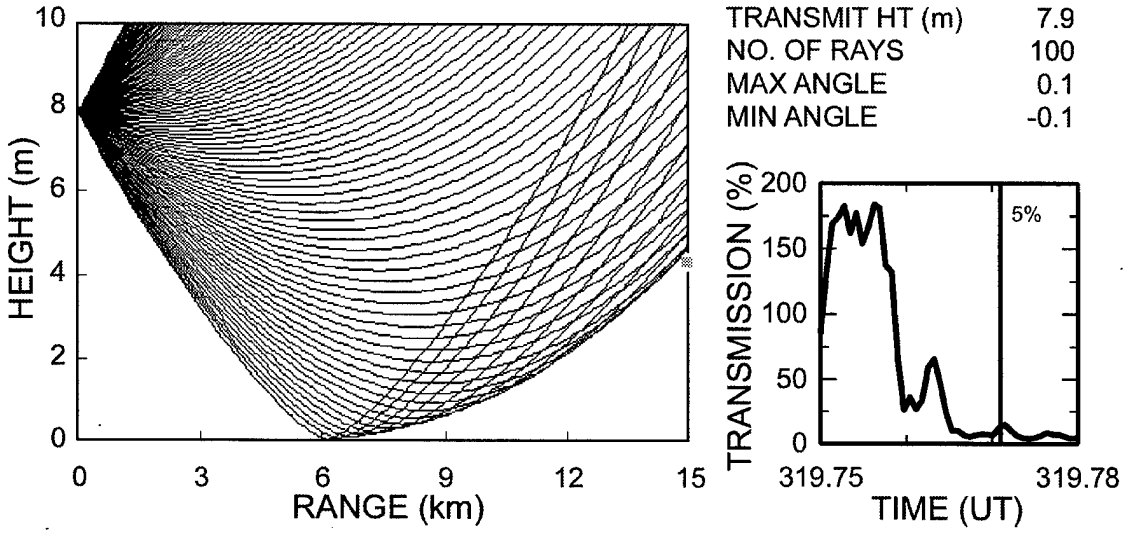

Figure 6. Flat-earth ray trace diagram for 100 rays launched from a transmitter at an altitude of 8 m above mean sea level towards a receiver. The receiver (gray dot) is 15 km away at an altitude of 4 m above mean sea level. The air–sea temperature difference is –1.7 °C. This trace was derived from a vertical profile of optical refractivity derived from similarity theory for the mean meteorological conditions prevailing at time 319.7708 in 1996. Note that no rays are able to reach the receiver; the receiver is below the horizon. The inset shows the transmission measured by TNO for nearby times. The vertical line denotes the exact time corresponding to the trace when the transmission was 1/20th of the free space value.

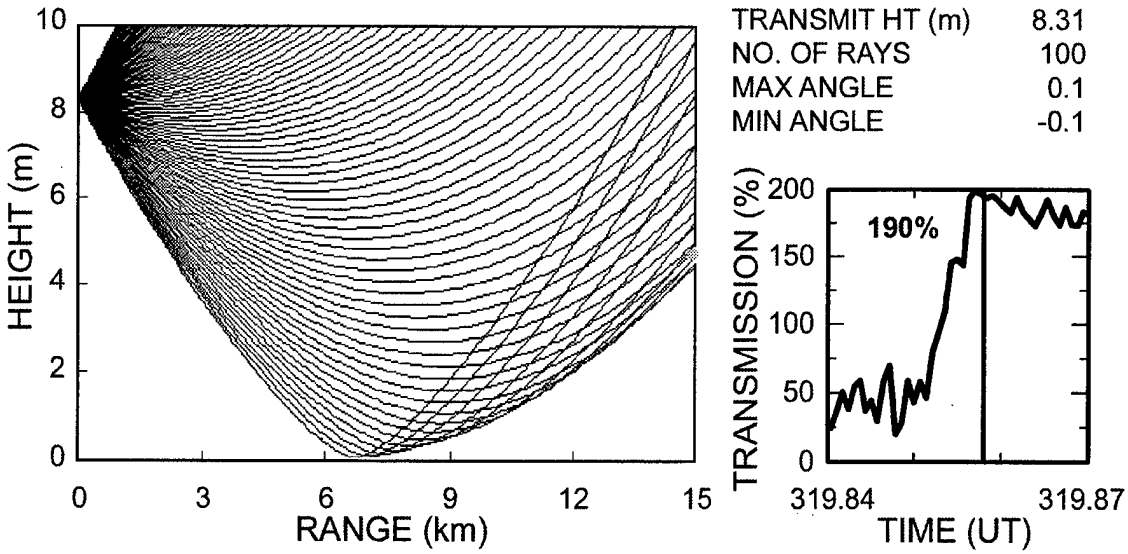

Figure 7. Similar to figure 6 except 2 hours later. The time is 319.8542. The air–sea temperature difference is now –1.4 °C, the tide has fallen by 40 cm, and the receiver is not only above the horizon, it is in a mirage. The inset shows the transmission measured by TNO at surrounding times. The vertical line indicates the exact time corresponding to the trace when the transmission was 1.9 times the free space-value.

2.4 TRANSMISSION: THE SIGNAL AVERAGE

Up to this point, we have implicitly been discussing the time-averaged value of the signal transmitted along an optical path. The field experiment provides a voltage (or current) time series. The time series has rapid random variations because of detector noise, slower random variations (of about 10 Hz) caused by scintillation, and slow (fractions of an hour) deterministic variations caused by changes in the atmosphere. (Scintillation, which will be discussed later, may be thought of as "atmospheric noise.") The slow variations are described by the word "transmission" and measured by averaging the time series over an interval long compared to the scintillation time and short compared to the time required for the atmosphere to change. Typically, an averaging time of 10 minutes is used to determine the mean.

After calibration, the mean value of the voltage time series can be converted into transmission, which we represent by the following expression combining all three of the effects previously discussed:

$$\tau = \tau_m \{r(v)\} \exp\{-\sigma_p(v) L\} F^2. \tag{5}$$

2.5 INTERFERENCE

Optical scintillation refers to the fluctuation of the signal about its mean value. Scintillation is caused by interference in the detector between two rays originating from the same point on the source. Ordinarily, two such rays would propagate radially away from one another and never meet on

the detector. However, random fluctuations in the index of the air continually occur, and it may happen that they momentarily bend the two diverging rays toward one another and cause them to meet briefly on the detector. Since they originated from the same point on the source, they are capable of interfering (even though the source is incoherent), which they may do destructively or constructively, depending on their relative phase. The twinkling of stars is caused by this phenomenon.

Scintillation measurements are made by recording a voltage (or current) time series. However, theoretical results in the turbulence literature are commonly expressed either in terms of $\sigma_{\ln I}^2$, the variance of the log-intensity, or in terms of σ_χ^2, the variance of the log-amplitude. The appendix shows that the experimental and theoretical quantities are related by

$$\ln\left(1+\frac{\sigma_V^2}{\mu_V^2}\right)=\ln\left(1+s_V^2\right)=\sigma_{\ln I}^2=4\sigma_\chi^2, \tag{6}$$

where the scintillation index, s_V^2, is the variance of the voltage time series, σ_V^2, divided by the square of its mean, μ_V. One over the square root of the scintillation index gives the signal-to-atmospheric noise ratio. When the scintillation index is less than about 1, the turbulence is called "weak" and the scintillation index is theoretically proportional to the square of the refractive index structure constant, C_n^2, defined (Andreas, 1988) by

$$\left\langle [n(\mathbf{x}+\mathbf{r})-n(\mathbf{x})]^2 \right\rangle = C_n^2\, r^{2/3}. \tag{7}$$

Here, n is the refractive index of the atmosphere, $\mathbf{x}$ and $\mathbf{r}$ are two points in space, r is the magnitude of $\mathbf{r}$, and the angular brackets denote a time average. The refractive index structure constant is the most important parameter characterizing the propagation of electromagnetic waves through a turbulent refractive medium.

2.6 SCINTILLATION: THE SIGNAL VARIANCE

According to the Rytov theory of weak turbulence (Hufnagel, 1989; Hill and Ochs, 1978), the scintillation index is

$$s_V^2 = \exp\left\{0.496 C_n^2\, k^{7/6}\, L^{11/6}\right\}-1 \approx 0.496 C_n^2\, k^{7/6}\, L^{11/6}, \tag{8}$$

where k is 2π divided by the optical wavelength, λ, and L is the range. Equation (8) refers to the case of a beam wave propagating horizontally from a point source through uniform weak turbulence to a point receiver. There is a modification to this result when the transmitter and receiver have finite apertures that spatially average the point intensity pattern. For equal transmitter and receiver diameters $D >> \sqrt{\lambda L}$, analysis by Hill and Ochs (1978) shows that equation (8) should be replaced by

$$s_V^2 = \exp\left\{0.9 C_n^2\, D^{-7/3}\, L^3\right\}-1 \approx 0.9 C_n^2\, D^{-7/3}\, L^3. \tag{9}$$

In the midwave band for a 20-cm instrument on a 7-km range, the coefficient of C_n^2 in equation (9) is about eight times less than the coefficient of C_n^2 in equation (6), so aperture averaging is an important feature of our instrument.

The quantity, $\sqrt{\lambda L}$, known as the Fresnel zone size, is the size of the most effective turbulent eddy along the path. In our instrument, the transmitter and receiver diameters are both 20 cm and the Fresnel zone sizes on a 7-km range are 27 cm in the longwave band and 16 cm in the midwave band. Therefore, we do not meet the requirements for application of equation (9), and we concede that it only approximates our situation. However, equation (9) is within several percent of the more complicated exact expression (Churnside, Lataitus, and Wilson, 1992) and is sufficiently accurate for the purpose of this report.

For a 7-km path, the midwave infrared scintillation index typically varies from 0.01 (signal-to-atmospheric noise 10/1) in very still conditions (a refractive index structure constant, C_n^2, of about 8 x 10^{-16} $m^{-2/3}$) to 0.3 (signal-to-atmospheric noise 2/1) in very turbulent conditions (C_n^2 about 2 x 10^{-14} $m^{-2/3}$). However, the signal-to-atmospheric noise situation in turbulence is actually worse than the signal-to-atmospheric noise ratio indicates because scintillation has a log normal spectrum with large spikes that commonly exceed the mean by five times the standard deviation.

Infrared scintillation frequencies are typically in the 10-Hz region, with maxima reaching 100 Hz (Clifford, 1971).

3. A TRANSMISSOMETER

From the previous discussion, it is evident that a transmissometer can measure transmission if it has a large enough signal-to-detector noise ratio at its intended range, and that it can measure scintillation if it has a detector noise variance significantly less than the expected atmospheric variance. Both transmitter and receiver must have a field of view of at least several mrad to accommodate typical refractive beam wander. For long ranges, all these requirements will be more restrictive than for short ranges.

We now discuss the instrument we have used to make measurements along a 7-km range across San Diego Bay. As figure 8 shows, the transmissometer consists of a transmitter and a receiver. In the transmitter, the aperture of a black body[1] is located in the focal plane of a Newtonian reflecting telescope. The primary mirror of the transmitter is a gold-coated paraboloid 20-cm in diameter with a focal length of 1.22 m (F/6). The diameter of the black body aperture is typically 6.3 mm in the field, giving a transmitter beam width of 5.3 mrad (full angle) and a footprint about 35 m in diameter when the receiver is 7 km away. The secondary mirror and its support obscure 5.8% of the primary area. The black body is operated at a temperature of 1200°K and chopped with a blade at a frequency of 1 kHz. A reference signal from the chopper blade is transmitted by a 160.1-MHz radio[2] signal to a synchronous detector (also called a lock-in detector) at the receiver. The receiver consists of a

---

[1] Model SR-20, manufactured by CI Systems, Incorporated, 5137 Clareton Drive, Suite 220, Agoura Hills, CA 92301.

[2] Model DR-150 VHF FM Transceiver, Alinco Electronics Incorporated, 438 Amapola Avenue, Suite 130, Torrance, CA 90501-6201.

nominally identical Newtonian telescope with a 5-mrad field of view. In the receiver, the secondary mirror and support obscure 12.1% of the primary area. After reflection at the secondary mirror, the beam passes through a coated ZnSe beam splitter that transmits 93% of the longwave band towards a HgCdTe detector and reflects 95% of the midwave band towards an InSb detector. A ZnSe field lens placed at the prime focus precedes each detector. Figure 9 shows a photograph of the receiver.

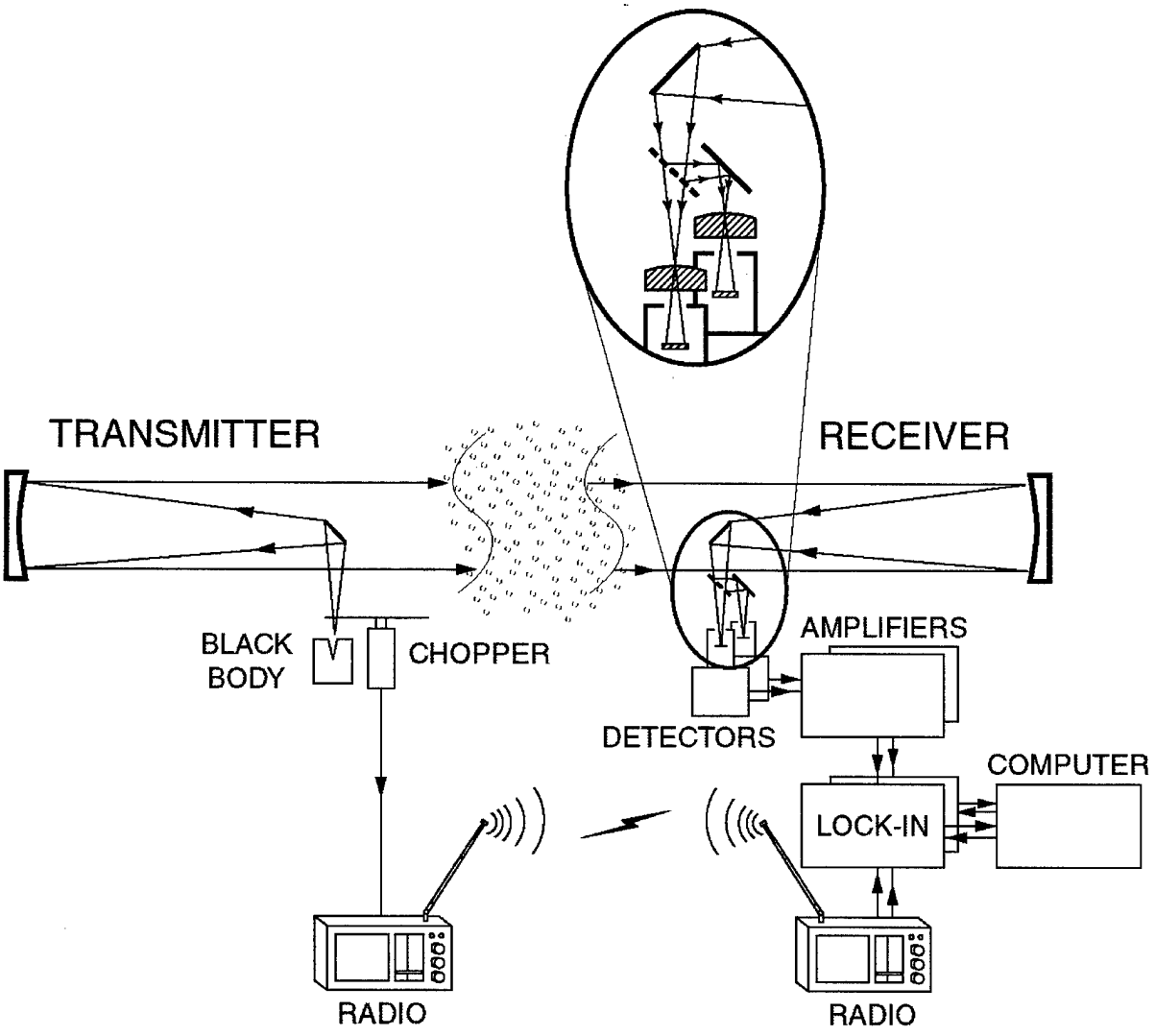

Figure 8. Schematic diagram of a broadband transmissometer. There are two discrete detectors, one for the midwave band and one for the longwave band. The expanded view shows the beam splitter (dashed line) and field lenses. Since each detector sees exactly the same path through the atmosphere, this instrument is suitable for measuring the correlation between the scintillation in the two bands. The lock-in wait time is typically set to 30 s for transmission and 10 ms for scintillation.

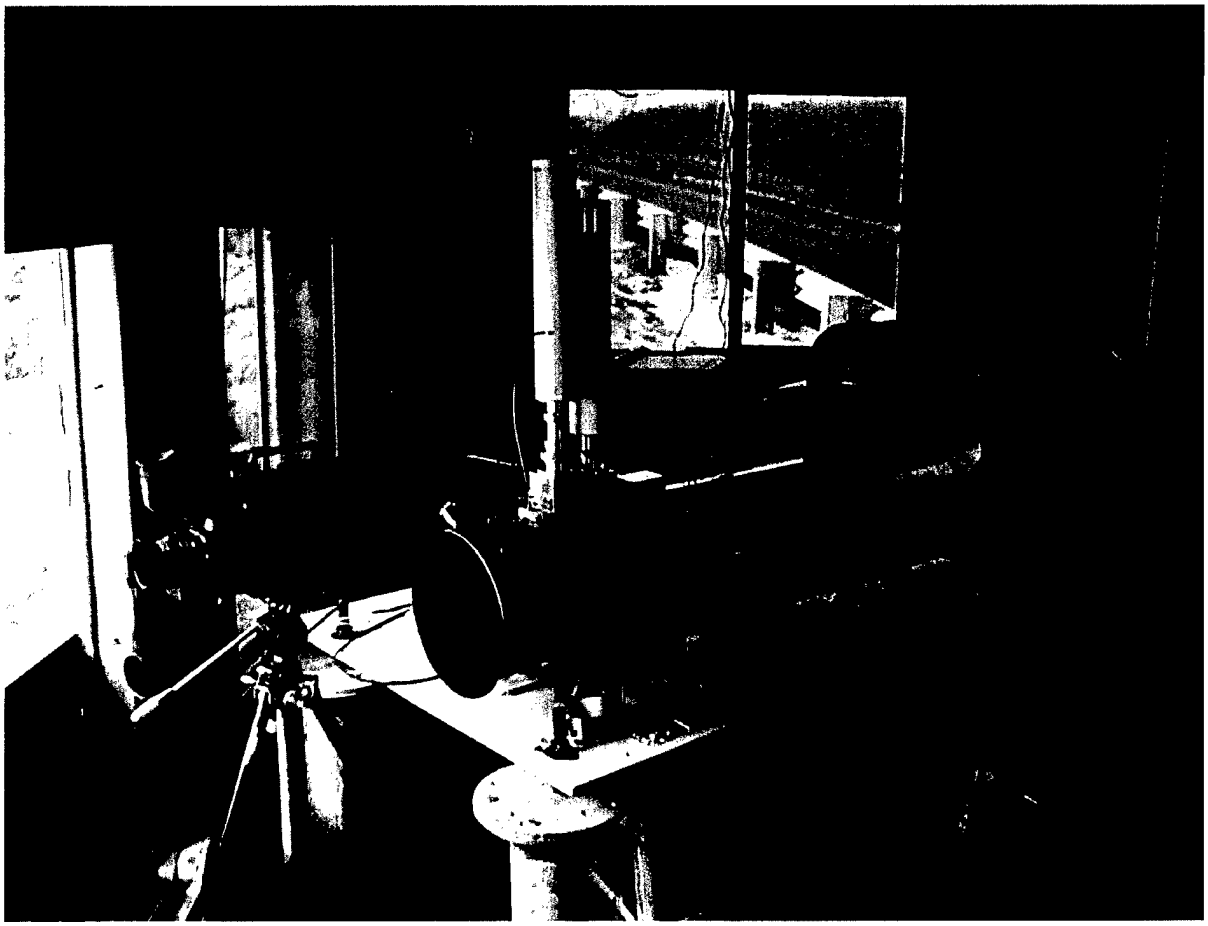

Figure 9. Receiver installed inside a trailer in the field. The 25-cm-diameter horizontal aluminum tube, in the foreground, supports the receiver primary and secondary mirrors (neither of which are visible in this photograph) as well as the two detector dewars, which are the two white cylinders, mounted vertically on the top left end of the aluminum tube. One of two cones for pointing the receiver is shown near the left front corner of the table. The table rests on three pipes that reach through holes in the floor to a concrete pad on the ground below.

3.1 FIELD LENS

A single ZnSe lens with a focal length of 8.89 mm collimates the light and forms a 1.46-mm-diameter exit pupil that is the real image of the entrance pupil. The detector is placed in the plane of the exit pupil and a point object source is imaged on it as a blur 1.46 mm in diameter. The object field of view received by the detector is determined by the cold-stop-acceptance angle divided by the angular magnification of the telescope. In both the longwave and midwave detectors the cold stop acceptance angle is 40.5 degrees (700 mrad) and this is divided by the angular magnification of 137, yielding an object field of view of 5 mrad.

The field lens serves several useful functions. It collects a larger field for the detector, in this case, 5 mrad compared to 1.7 mrad if the detector is placed at the prime focus. This makes the receiver less sensitive to pointing errors and refractive wander (as the upper part of figure 5 shows). Since the

detector is at the exit pupil, the location of the blur on the detector stays the same regardless of the location of the source within the field of view (5 mrad). This large and unmoving blur averages out detector non-uniformity. Conversely, with the detector at the prime focus, a point would be imaged as point, with an image location directly coupled to the object location, making the detected signal sensitive to local variations across the detector. Finally, the field lens vastly improves the cold-stop efficiency. In the simple case of a detector at the prime focus, the detector field of view would be dominated by the interior of the receiver housing because while the detector cold-stop field of view is 40.5 degrees, the objective covers only 9.5 degrees of that field. (i.e., a cold-stop efficiency of only 5.5% by area). With the field lens, the entrance pupil is matched to the cold stop, producing almost 100% efficiency.

3.2 DETECTORS

The detectors are discrete (non-imaging) devices cooled to 77 °K. For a given source radiance, set by the 1200°K temperature of the black body, the detector responsivity, detector noise, and lock-in bandwidth determine the signal-to-detector noise ratio in the field. Table 1 shows the limitation imposed by detector noise for operation on a 7-km range. Detector noise and the A/D level are given as a per cent of the 7-km free-space signal. In this instrument, longwave scintillation is severely limited at a 7-km range by detector noise; when the longwave transmission is 10% of free space, the signal-to-detector noise ratio is only 3 to 1.

3.2.1 Longwave

The longwave detector[3] is a 2-mm-square HgCdTe photoconductor mounted below a cold optical filter that has an approximately square passband between 872 and 1023 cm^{-1}. Figure 10 shows the relative spectral responsivity of the longwave detector-filter combination. The detector and filter were mounted 5 mm below a warm ZnSe window. The detector field of view was 90° (full angle) and the detector resistance was 254 ohms at 77°K. The responsivity was 390 V W^{-1} per mA of bias current. The responsivity varied with room temperature at the rate of -2% per °C. After correction for this variation, stability was better than 2% per day. The in-phase noise was 2.0 nV $Hz^{-1/2}$ per mA of bias current. This noise arose from 1/f noise combined with noise caused by generation and recombination noise at background impurities in the HgCdTe material. The detector was

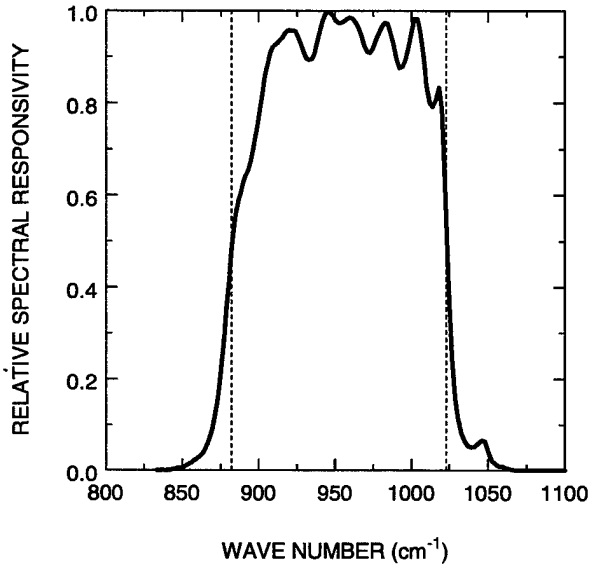

Figure 10. Combined relative spectral responsivity of the longwave detector and filter. The vertical dashed lines at 882 and 1023 cm^{-1} show the 50% response points.

[3]EG&G Judson Optoelectronics, 221 Commerce Drive, Montgomeryville, PA 18936.

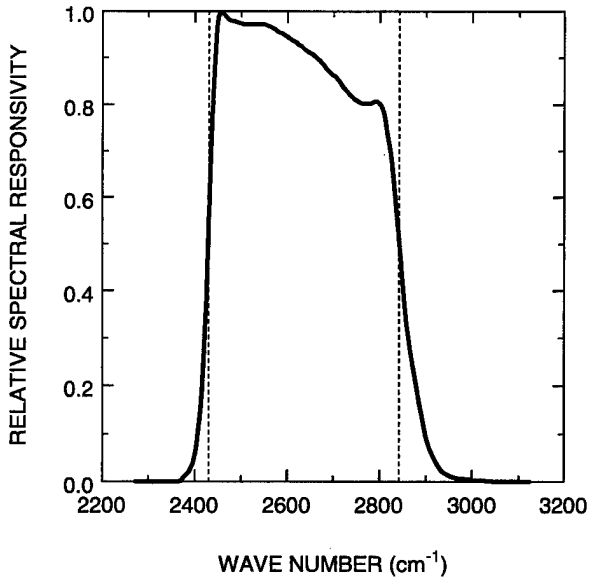

Figure 11. Combined relative spectral responsivity of the midwave detector and filter. The vertical dashed lines at 2430 and 2842 cm^{-1} show the 50% response points.

supplied with current by a 15-V NiCd battery in series with a 1990-ohm resistor.

3.2.2 Midwave

The midwave detector[3] is a 2-mm-diameter circular InSb photodiode mounted below a cold optical filter that had an approximately square passband between 2430 and 2842 cm^{-1}. Figure 11 shows the relative spectral responsivity of the midwave detector-filter combination. The detector and filter were mounted 5 mm below a warm sapphire window. The detector field of view was 90° (full angle). The detector responsivity was 2.9 A W^{-1} and the in-phase noise was 3.5 pA per root Hz (limited by pickup). The detector was linear to better than ±2% for incident optical power ranging over three orders of magnitude from 0.1 to 100 nW_{rms}. After correcting for a temperature dependence to the responsivity of -0.65% per degree Centigrade, stability was better than 0.6% per day.

3.3 ELECTRONICS

A pre-amplifier and a lock-in followed each detector. The lock-in output was sampled with a bipolar 12-bit analog-to-digital converter and the lock-in roll-off was set to 24-dB $octave^{-1}$ (four poles). The longwave pre-amplifier was a voltage amplifier with a nominal gain of 1000X. The midwave pre-amplifier was an operational amplifier with a 10^5-ohm feedback resistor followed by a voltage amplifier with a nominal gain of 10X.

3.4. OPERATING CHARACTERISTICS

Figure 12 shows the spectral distributions of the source, atmosphere, and detectors. The signal is proportional to the integrated product of the three curves. Transmission is measured by setting the lock-in detector to a slow time constant and scintillation is measured by setting it to a fast time constant. Separate detectors mounted on the same receiver provide an identical optical path in each band when correlating the scintillation between the bands.

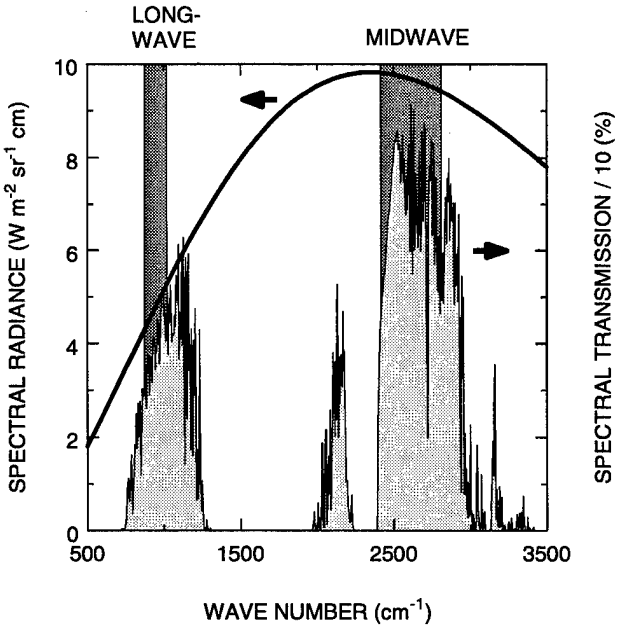

Figure 12. Overall spectral behavior of the transmissometer. The thick solid line shows the spectral radiance, on the left ordinate, of the 1200°K black body source. The light gray area under the thin solid line shows, on the right ordinate, the spectral transmission of the atmosphere after division by 10. The dark vertical bars indicate the relative spectral responsivities of the longwave and midwave detector-filter pairs (shown in greater detail in figures 10 and 11 respectively).

4. CALIBRATION

The transmissometer is calibrated with a zero-range laboratory measurement. The calibration does not depend on knowing the detector responsivity or the optical properties of any of the mirrors or lenses in the instrument. (Optical infrared properties are somewhat difficult to measure accurately.)

The method relies on the law of conservation of radiance (Friberg, 1981; Wolf, 1978) and three assumptions:

1. The detector signal is linearly proportional to the optical power falling on the detector,
2. The image of the source underfills the detector in the lab and in the field, and
3. Nothing changes between the lab and the field except the range, the temperature of the black body, and the size of the black body aperture.

In the laboratory, the transmitter and receiver telescopes face one another, separated by a fraction of a meter. The temperature of the black body is set to T_o and the area of the black body aperture is set to A_o. Let the spectral radiance of a black body at temperature, T_o, be $B\{T_o, \nu\}$, and let the broad band spectral radiance of that black body in the detector spectral band, $r(\nu)$, be $B\{_o, r(\nu)\}$, defined by an equation similar to equation (1). Furthermore, let the optical throughput (the combined in-band transmission and reflection of all optical elements) be ρ, let the focal length of the transmitting primary be f, let the clear area of the collimated beam between transmitter and receiver be A, and let the in-band atmospheric transmission be τ_o. The root-mean-square (rms) laboratory voltage, V_o, will be equal to the detector responsivity, $\Re$, times the peak-to-peak laboratory power, P_o, and can be calculated from the radiance at the black body aperture according to

$$V_o = \Re F_o P_o = \Re F_o B\{T_o, r(\nu)\} A_{bb} \frac{A}{f^2} \rho \, \tau_o. \qquad (10)$$

In this equation, F_o is the laboratory blade factor[4] (Hudson, 1969).

In the field, the transmitter and receiver still face one another but are now separated by the full range, L. We now set the black body temperature to T and widen the black body aperture diameter to about 6 mm. Let the clear area of the transmitter primary be A_{Tx}, let the clear area of the receiver primary be A_{Rx}, and let the in-band atmospheric transmission be τ. The rms field voltage, V, will be equal to the detector responsivity, $\Re$, times the peak-to-peak field power, P, and can be found from the radiance at the transmitter primary according to the following expression:

$$V = \Re F P = \Re F B\{T, r(v)\} A_{Tx} \frac{A_{Rx}}{L^2} \rho \tau \equiv V_{fs} \tau, \tag{11}$$

that also serves to define the free-space voltage, V_{fs},. In equation (11), the symbol V really stands for μ_v, the (usually 10-minute) mean value of the voltage time series.

We want a calibration procedure that does not require knowledge of $\Re$ and ρ. We eliminate them by taking the ratios of equations (11) and (10) to get

$$\frac{V}{V_o} = \frac{\tau V_{fs}}{V_o} = \frac{F}{F_o} \frac{B\{T, r(v)\}}{B\{T_o, r(v)\}} \frac{A_{Tx} A_{Rx}}{A_o A} \left(\frac{f}{L}\right)^2 \frac{\tau}{\tau_o}. \tag{12}$$

By choosing optical filters inside an atmospheric transmission band that are narrow enough to avoid strong absorption regions (such as the CO_2 region at 2300 cm^{-1}) but still wide enough to maintain a strong signal, we can arrange that τ_o equal unity. Then the atmospheric transmission at full range will be given by

$$\tau = \frac{V}{V_{fs}}, \tag{13}$$

where

$$V_{fs} = \frac{F}{F_o} \frac{B\{T, r(v)\}}{B\{T_o, r(v)\}} \frac{A_{Tx} A_{Rx}}{A_o A} \left(\frac{f}{L}\right)^2 V_o \tag{14}$$

is the free-space voltage that can be modeled by means of equation (11) or calculated and measured by means of equation (14). Typical values for the quantities appearing in equation (14) are listed in table 2.

Note that the field voltage given by equation (11) is independent of the black body aperture (except for its minor role in determining the blade factor). The black body aperture is widened in the field merely to accommodate refractive wander of the beam footprint at the receiver.

---

[4] The chopper blade factor, determined by the relative sizes of the black body aperture and the chopper blade, is the ratio of the peak-to-peak value of the signal to the rms value of its first harmonic.

5. LIMITATIONS OF THE INSTRUMENT

5.1 ABSOLUTE ERROR

We estimated random and systematic errors in the calibration and operation of the transmissometer. (Accuracy applies only to the transmission measurement; scintillation is a relative measurement.) The errors fall into three categories: (1) measurement uncertainty connected with a calibration quantity appearing in equation (14), (2) non-uniformity of an optical component, and (3) instability of an optical or electronic component. Table 3 lists these errors and shows that the absolute accuracy is ±7% in each band. This accuracy is limited primarily by our inability to precisely align the transmitter and receiver primary mirrors during calibration. Allowing for systematic errors that we may have overlooked, we adopt an absolute accuracy of ±10% for this instrument.

5.2 REFRACTION

Equation (4) shows that the field of view required for reliable operation will be proportional to range. Experience indicates that the 5-mrad field in our instrument may not be large enough for ranges approaching and exceeding 20 km.

5.3 FORWARD SCATTERING BY AEROSOL PARTICLES

The receiver will measure any radiation in its field of view with wave numbers in the detector passband. The simplest interpretation of the received signal would be that it originated from the direct, unscattered radiation emitted by the source. This interpretation neglects mirage and reflected rays and assumes that all of the radiation scattered by aerosol particles is completely lost. However, it is not completely lost; some of it is scattered in the forward direction (Chu and Hogg, 1968). This introduces an error that we will now estimate. We will neglect multiple scattering in our estimate. We will assume a uniform distribution of aerosol particles along the entire path.

Figure 13 shows a transmitter and receiver, each with its own active area, A, and angular field, θ (full angle). To be effective in scattering radiation into the receiver, particles must be irradiated by the transmitter and viewed by the receiver. That means that they must lie in the intersection of the two conical fields shown in figure 13. Aerosol particles located there scatter an amount of radiation given by the volume angular scattering coefficient (McCartney, 1976):

$$\beta_p(\nu,\theta)=\frac{1}{V}\frac{J(\nu,\theta)}{H}=\frac{1}{2k^2}\int_0^\infty\{i_1(\nu,r,\tilde{n},\theta)+i_2(\nu,r,\tilde{n},\theta)\}\frac{dN}{dr}dr. \qquad (15)$$

This coefficient gives the intensity of radiation, J, scattered in the direction, θ, away from the forward direction by a polydispersion of particles located in volume, V, and exposed to an irradiance, H. The intensity functions, i_1 and i_2, are provided by Mie theory. Equation (15) holds for unpolarized radiation.

Consider an incremental disk of scattering particles located a distance, x, from the transmitter. Let l be the distance from the transmitter to the widest part of the scattering volume. The disk has a volume

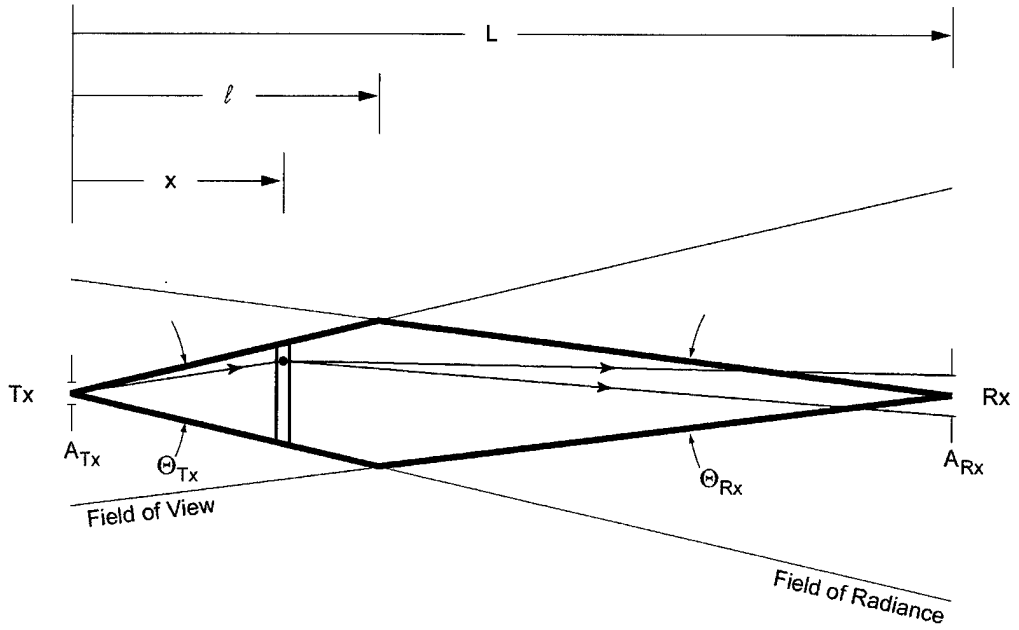

Figure 13. Geometry pertaining to forward scattering by aerosol particles. Particles that contribute to the effect must be located inside the intersection of two cones. This intersecting volume is widest at the distance, *l*, from the transmitter. A single particle, contained in an incremental disk located a distance, *x*, from the transmitter, is shown scattering radiation into the receiver located a distance, $L - x$, from the particle.

of

$$\begin{aligned} V(x) &= \frac{\pi}{4}\theta_{Tx}^2\, x^2 dx, \quad x \le l \\ &= \frac{\pi}{4}\theta_{Rx}^2\, (L-x)^2\, dx, \quad x > l, \end{aligned} \tag{16}$$

receives an irradiance of

$$H(x) = \frac{B\, A_{Tx}}{x^2}, \tag{17}$$

and scatters the following amount of power forward into the receiver:

$$P_{sc}(x) \approx J(v,0)\frac{A_{Rx}}{(L-x)^2} = \beta_p(v,0)V(x)H(x)\frac{A_{Rx}}{(L-x)^2}. \tag{18}$$

The total power scattered into the receiver by all effective particles is given by integrating the scattered power along the entire path:

$$
\begin{aligned}
P_{sc} &\approx \int_0^L P_{sc}(x)dx \\
&= \beta_p(\nu,0)\left\{B\,A_{Tx}\frac{A_{Rx}}{L^2}\right\}\frac{\pi}{4}L^2\left[\int_0^l \frac{\theta_{Rx}^2}{(L-x)^2}dx+\int_l^L \frac{\theta_{Tx}^2}{x^2}dx\right] \\
&= \beta_p(\nu,0)\left\{B\,A_{Tx}\frac{A_{Rx}}{L^2}\right\}\frac{\pi}{4}L^2\left[\frac{\theta_{Rx}^2}{L}\int_0^{u'}\frac{du}{(1-u)^2}+\frac{\theta_{Tx}^2}{L}\int_0^{u'}\frac{du}{u^2}\right] \\
&= \beta_p(\nu,0)\left\{B\,A_{Tx}\frac{A_{Rx}}{L^2}\right\}\frac{\pi}{4}L^2\left[\frac{2}{L}\theta_{Tx}\theta_{Rx}\right],
\end{aligned}
\tag{19}
$$

$$
u \equiv \frac{x}{L},
$$

$$
u' \equiv \frac{l}{L} = \frac{\theta_{Rx}}{\theta_{Rx}+\theta_{Tx}}.
$$

This result can be brought into a more useful form by noting that: (1) the quantity in curly brackets is the power, P_{fs}, that would be received by an ideal instrument in free space, (2) the integral of the angular scattering coefficient over all angles is equal to the total scattering coefficient, $\beta_p(\nu)$, and (3) $\beta_p(\nu,\theta)$ is related to the phase function, $\Phi(\nu, \theta)$, by

$$
\Phi(\nu,\theta) = \frac{\beta_p(\nu,\theta)}{\beta_p(\nu)}. \tag{20}
$$

We note that the integral of the phase function over all solid angles is one. With this normalization of the phase function, $\Phi(\nu,\theta)d\omega$ is the fraction of radiation that is scattered into a solid angle, $d\omega$, about an angle, θ, relative to the incident radiation. Making these substitutions, we have a fractional forward scattering error of

$$
\begin{aligned}
\frac{P_{sc}}{P_{fs}} &\approx \Phi(\nu,0)\frac{\pi}{2}\theta_{Tx}\theta_{Rx}\beta_p(\nu)L \\
&\le \Phi(\nu,0)\frac{\pi}{2}\theta_{Tx}\theta_{Rx}\sigma_p(\nu)L = -\Phi(\nu,0)\frac{\pi}{2}\theta_{Tx}\theta_{Rx}\ln(\tau_p)
\end{aligned}
\tag{21}
$$

that is our final result. In equation (21), the total scattering coefficient has been replaced by the total extinction coefficient (i.e., there is no absorption, or equivalently, the single scattering albedo is one). This gives an upper limit to the scattered power ratio. Also, equation (3) expresses the upper limit as measured aerosol transmission.

Having finished our derivation, we must point out that the description of the scattering volume we have given is only an approximation. There is actually a transition region surrounding the scattering volume where the irradiance falls monotonically to zero (Boyd, 1983). Since the lateral distance of the transition region is on the order of the instrument diameter, the volume of the transition region is small in comparison with the central volume, and we are justified in neglecting it. Furthermore, we

have assumed in equation (18) that the forward lobe of the phase function, no matter how sharply peaked, is constant over the forward scattering angle. This approximation is also a good one because typical forward lobes have widths of tens of mrad. These widths are large compared to the small angles subtended by the instrument aperture at particle locations along the range.

Our result shows that the larger the aerosol extinction, the larger the forward scattering and the larger the forward scattering error. According to equation (21), an instrument with equal transmitting and receiving fields of 5 mrad (full angle) measuring an aerosol transmission of 10% (1%) would suffer a 1% error if the forward lobe of the phase function for the polydispersion reached 110 (55). It is well-known that the forward scatter lobe increases with the Mie parameter, $x \equiv k\,r$, where r is the radius of the aerosol particle. Hence, the forward lobe (and the error) will be largest for large particles (e.g., fog) and small wavelengths. At wavelengths in the longwave and midwave bands, ocean aerosol distributions have phase function forward lobes that range from 1 to 10 and fogs have phase function forward lobes that range from 50 to 150 (Kneizys et al., 1983.)[5]

From these results, it seems likely that the error caused by particle forward scattering would normally be on the order of 0.1% or less, but that it might rise to 1% when there is fog.

5.4 MAXIMUM RANGES

We now estimate the maximum useful range in each of the two measurement modes. Let

$$G_\tau \equiv \frac{S_\tau}{N} = \frac{V}{V_n\sqrt{\Delta f}} = \frac{\tau V_{fs}}{V_n\sqrt{\Delta f}} \tag{22}$$

be the signal-to-detector noise ratio in transmission mode. Here, the numerator is the mean value of the voltage waveform, μ_v, and it can be obtained in two ways: either by use of equation (14) together with a laboratory calibration, or by use of equation (11) together with a measurement of $\Re$ and ρ. The calibration is more accurate, but we will use equation (11) because it is more descriptive. Substituting equation (11) into equation (22) and rearranging terms, we arrive at

$$L_\tau^2 = \frac{\Re F\, B\, A_{Tx} A_{Rx} \rho}{G_\tau V_n \sqrt{\Delta f}}\,\tau \tag{23}$$

for the range associated with a particular signal-to-detector noise ratio. However, equation (23) is inadequate as it stands because it contains atmospheric transmission that itself depends strongly on range. Given the complicated effects described earlier, what shall we adopt for this range dependence? Our arbitrary but simple answer is a Beer's Law approximation to molecular transmission. This means that our criterion for maximum useful range will be the ability to measure clear air transmission with a given signal-to-detector noise ratio. We then have the following transcendental equation for maximum useful transmission range:

---

[5] The phase functions tabulated (Kneizys et al., 1983) are normalized such that their integral over all solid angles is one.

$$L_\tau^2 \exp(\beta_m L_\tau) = \frac{\Re F B A_{Tx} A_{Rx} \rho}{G_\tau V_n \sqrt{\Delta f}}, \tag{24}$$

where $\beta_m \equiv \beta_m[r(\Delta\nu)]$ is the broadband molecular extinction coefficient for an instrument with the relative spectral responsivity, $r(\Delta\nu)$. Using the values given in tables 1 and 2, adopting 10 to 1 for a signal-to-detector noise ratio, and estimating a molecular extinction by replacing each curve in figure 2 with a straight line, we find a maximum transmission range of about 18 km in the longwave and 90 km in the midwave.

Next, let

$$G_\chi \equiv \frac{S_\chi}{N} = \frac{\sigma_V}{V_n \sqrt{\Delta f}} \tag{25}$$

be the signal-to-detector noise ratio in scintillation mode. Here, the numerator is the standard deviation of the voltage waveform, σ_v, which can be obtained via equation (9) when aperture averaging is important. Substituting the approximate form of equation (9) into equation (25), and using

$$\mu_V = \tau V_{fs} \tag{26}$$

with equation (11) for V_{fs}, we arrive at

$$L_\chi^{1/2} = \frac{\Re F B A_{Tx} A_{Rx} \rho \sqrt{0.9 C_n^2 D^{-7/3}}}{G_\tau V_n \sqrt{\Delta f}} \tau \tag{27}$$

for the range associated with a particular signal-to-detector noise ratio in the scintillation mode. Adopting the Beer's Law approximation in figure 2 once again for τ, we obtain

$$L_\chi^{1/2} \exp(\beta_m L_\chi) = \frac{\Re F B A_{Tx} A_{Rx} \rho \sqrt{0.9 C_n^2 D^{-7/3}}}{G_\tau V_n \sqrt{\Delta f}}. \tag{28}$$

Assuming quiet air for which C_n^2 is 1 x 10^{-16} $m^{-2/3}$ and still using 10 to1 as a minimum useful signal-to-detector noise ratio, we find a maximum scintillation range of only 100 m in the longwave, but 20 km in the midwave.

Our instrument is obviously unsuitable for measuring scintillation in the longwave band. There are three reasons for such poor longwave scintillation performance: (1) low molecular transmission, (2) noisy detection, and (3) a weak source. Nothing can be done about the first reason, and not much can be done about the second. Although material impurities and 1/f noise currently limit our longwave detector, table 1 shows that the detector could be improved by a factor of only three before reaching the fundamental limit of infrared background noise. This threefold improvement would, however, push the maximum longwave scintillation range out to 1 km. The real solution to poor longwave scintillation performance is to provide a more radiant source, such as a laser.

5.5 TRANSMISSION RESOLUTION

If the separation between telescopes is fixed, the minimum resolvable change in transmission, $\Delta\tau$, is determined by the larger of the detector noise and the A/D converter resolution. If the limit is detector noise, then the resolution is equal to the value of τ satisfying equation (23) when G_τ is equal to one:

$$\Delta\tau = \frac{V_n\sqrt{\Delta f}\,L^2}{\Re F\,B\;A_{Tx}A_{Rx}\rho}. \tag{29}$$

For our instrument at a range of 7 km, table 1 shows that detector noise is comparable to the A/D resolution in the longwave and less than the A/D resolution in the midwave. Taking both limits into account, the resolution is about 0.1% in each of the bands at a range of 7 km.

6. ADDITIONAL CONSIDERATIONS

The receiver and transmitter must be mounted on stable supports so they can be pointed towards one another at the beginning of the experiment and occasionally adjusted subsequently. Small bore-sighted telescopes help optical alignment in the field. Alternatively, the objects (black body, field-lens-detector assembly) in the focal planes may be removed and temporarily replaced with telescope objectives of a convenient magnification. When the far end of the range is seen through the objective, then the original equipment may be replaced, taking care that the mount is not moved in the process.

The transmitter and receiver must be shielded from the wind and weather, and the optical surfaces must be kept dry. (Wind is capable of cooling the black body cavity and changing its temperature, and condensation on the optics will strongly attenuate the signal.) The transmitter is generally installed, aligned, and secured in a single operation that takes about 12 hours if a shelter has already been prepared and supplied with electrical power. Thereafter, the transmitter seldom needs further adjustment or attention. The residual heat from the electronics and black body keeps the inside of the transmitter shelter 5 to 10°C above the outside temperature; as a consequence the interior of the shelter also stays dry.

The receiver requires regular attention, however. The data stream must be continually maintained. (Uninterruptable power supplies at both ends of the range help maintain the data stream.) The detector dewars must be regularly supplied with LN_2, and a hold-time a few hours beyond 24 makes this regular task much less of a chore. (We avoided the use of automatic LN_2 filling devices; they shook the receiver out of alignment.) Useful accessories at the receiver end are a time-lapse video camera (to record weather conditions such as rain and fog), binoculars (for convenient observation of the transmitter and its surroundings), a telescope (for visual checks of refractive bending), and an extra computer (for performing calculations without interrupting the computer dedicated to taking data).

Although a transmissometer is sufficient for collecting data, it is insufficient for interpreting data. Successful interpretation requires knowledge of meteorological and aerosol properties along the optical path. Clearly, the generation of marine aerosols depends on the interaction between the wind and the waves. The calculation of the particle size distribution in the Navy Aerosol Model (Gathman,

1983), for example, uses the instantaneous and 24-hour average wind speed as two of its empirical parameters. The refractive effects of the atmosphere arise from the refractivity gradients caused by heat flux. The temperature gradients can be calculated from point measurements of relative humidity, temperature, pressure, and wind speed using similarity theory (Liu et al., 1979). The air–sea temperature difference is a particularly important parameter of atmospheric stability. Obviously then, it is necessary to measure at least the bulk meteorological parameters in the interpretation of transmission and scintillation data.

During our experiments, a buoy instrumented by the Naval Postgraduate School, Monterey, California, was anchored midway between the transmitter and the receiver. It measured the bulk meteorological parameters of the atmosphere near the sea surface. Wind speed and direction were measured at a height of 4.88 m. Relative humidity and temperature were measured at a height of 4.09 m and the sea-surface temperature was measured remotely from a height of 1.82 m. Barometric pressure was measured at 0.38 m. These measurements were usually collected every minute and later averaged over 10-minute intervals.

7. MEASUREMENT EXAMPLES

Figure 14 shows 2 days of transmission data taken with the transmissometer described in this report. These data were taken on a 7-km range across San Diego Bay on 4 and 5 September 1998, days 247 and 248 of that year. The lock-in time constant was 3 s with a roll-off of 24 dB per octave (a wait time[6] of 30 s), and the lock-in output was sampled once a minute (0.0167 Hz). These data were not further averaged and figure 14 shows every tenth point. Isolated low signals that occur simultaneously in each band are probably ships that block this low-altitude optical path.

Figures 15, 16, and 17 show 2 seconds of scintillation data taken by widening the electronic bandwidth of the lock-in. These data were taken on the same range at 0020 UT 11 September 1998 and 0800 UT 17 September 1998. Figure 15 shows midwave scintillation on each of these days. Figure 16 shows longwave scintillation on 17 September. Figure 17 shows longwave scintillation on 11 September. The lock-in time constant was 1 ms with a roll-off of 24 dB per octave (a wait time of 10 ms), and the lock-in output was sampled once every 2.5 ms (400 Hz). 11 September was very quiet: the scintillation index was 0.00134, corresponding to a value for C_n^2 of 1.01×10^{-16} $m^{-2/3}$. 17 September was very turbulent: the scintillation index was 0.139, corresponding to a value for C_n^2 of 9.82×10^{-15} $m^{-2/3}$.

[6] The wait time is the time required for the lock-in to reach 99% of a step change at its input.

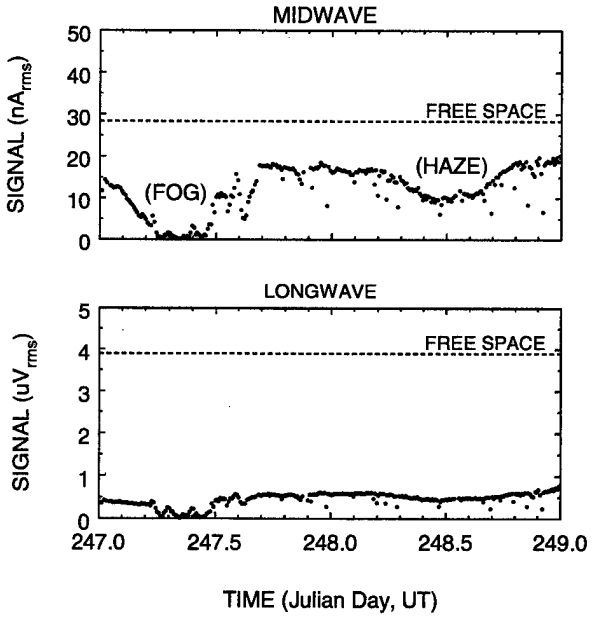

Figure 14. Two days of transmission data acquired on a 7-km range across San Diego Bay.

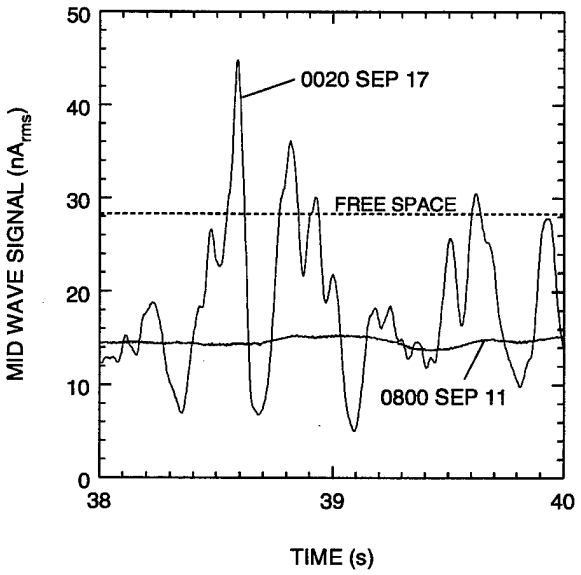

Figure 15. Two seconds of midwave scintillation data acquired on a 7-km range across San Diego Bay.

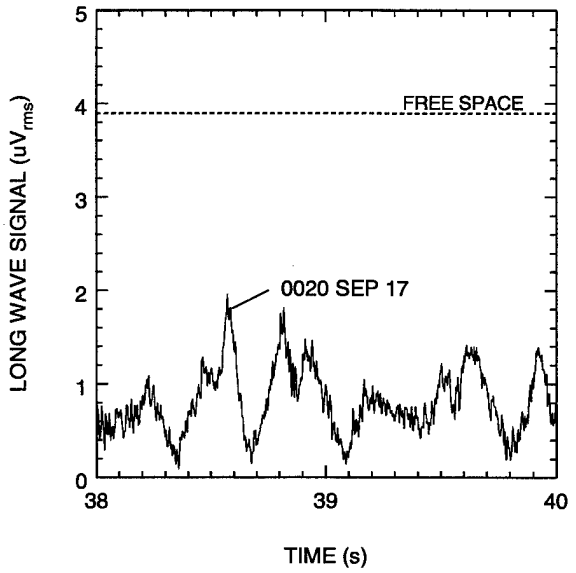

Figure 16. Two seconds of longwave scintillation data acquired on a 7-km range across San Diego Bay. (0020 17 September).

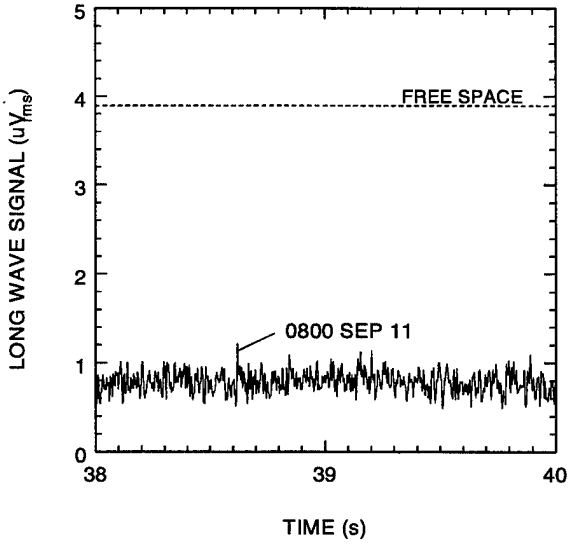

Figure 17. Two seconds of longwave scintillation data acquired on a 7-km range across San Diego Bay. (0800 11 September).

8. CONCLUSION

We have described a transmissometer that measured transmission (Zeisse et al., 1998) and scintillation (Frederickson et al., 1998) in the longwave and midwave infrared window regions. Our measurements took place in a coastal environment over a distance of 7 km for periods of several weeks. At this range, the transmission resolution is 0.1% in each band. It is possible to extend this range at the expense of reduced resolution. The maximum acceptable transmission range is about 18 km, limited by source radiance and longwave detector noise. The maximum acceptable scintillation range is about 20 km for the midwave channel. Longwave scintillation measurements are not practical with this instrument because it has a rather weak source, a black body.

Absolute transmission measurements can be made with 10% accuracy provided calibration measurements are taken before and after a measurement session. The equipment can be operated for extended periods (months) provided regular calibration checks are made.

9. REFERENCES

Andreas, E. L. 1988. "Estimating C_n^2 Over Snow and Sea Ice from Meteorological Data," *Journal of the Optical Society of America*, vol. A5, pp. 481–495.

Berk, A., L. S. Bernstein, and D. C. Robertson. 1989. "MODTRAN: A Moderate Resolution Model for LOWTRAN 7," Technical Report GL–TR–89–0122, Air Force Geophysics Laboratory, Hanscom Air Force Base, MA.

Boyd, R. W. 1983. *Radiometry and the Detection of Optical Radiation*. Wiley, New York, NY, p. 86 ff.

Chu, T. S. and D. C. Hogg. 1968. "Effects of Precipitation on Propagation at 0.63, 3.5, and 10.6 Microns," *Bell System Technical Journal*, vol. 47, pp. 723–759.

Churnside, J. H., R. L. Lataitis, and J. J. Wilson. 1992. "Two-color Correlation of Atmospheric Scintillation," *Applied Optics*, vol. 31, pp. 4285–4290.

Clifford, S. F. 1971. "Temporal-frequency Spectra for a Spherical Wave Propagating through Atmospheric Turbulence," *Journal of the Optical Society of America*, vol. 61, pp. 1285–1292.

Evans, M., N. Hastings, and B. Peacock. 1993. *Statistical Distributions*, p. 102, Second edition. Wiley, New York, NY.

Frederickson, P. A., K. L. Davidson, C. R. Zeisse, and C. S. Bendall. 1998. "Estimating the Refractive Index Structure Parameter (C_n^2) over the Ocean using Bulk Methods," In *Proceedings of the 1997 Battlespace Atmospherics Conference*, Technical Document 2989, pp. 571–578, K. D. Anderson and J. H. Richter, Eds. SSC San Diego, CA.

Freehafer, J. E., W. T. Fishback, W. H. Furry, and D. E. Kerr. 1951. "Theory of Propagation in a Horizontally Stratified Atmosphere." In *Propagation of Short Radio Waves*, p. 35, D. E. Kerr Ed. McGraw-Hill, New York, NY.

Friberg, A. T. 1981. "On the Generalized Radiance Associated with Radiation from a Quasihomogeneous Planar Source," *Optica Acta*, vol. 28, pp. 261–277.

Gathman, S. G. 1983. "Optical Properties of the Marine Aerosol as Predicted by the Navy Aerosol Model," *Opt. Eng.* vol. 22, pp. 57–62.

Hill, R. J. and G. R. Ochs. 1978. "Fine Calibration of Large-aperture Optical Scintillometers and an Optical Estimate of Inner Scale Turbulence," *Applied Optics*, vol. 17, pp. 3608–3612.

Hill, R. J., S. F. Clifford, and R. S. Lawrence. 1980. "Refractive-index and Absorption Fluctuations in the Infrared Caused by Temperature, Humidity, and Pressure Fluctuations," *Journal of the Optical Society of America*, vol. 70, pp. 1192–1205.

Hudson Jr., R. D. 1969. "Infrared System Engineering" p. 323 ff. Wiley, New York, NY.

Hufnagel, R. E. 1989. "Propagation through Atmospheric Turbulence." In *The Infrared Handbook*, chapter 6, W. L. Wolfe and G. J. Zissis, Eds. Revised ed. Environmental Research Institute of Michigan, Ann Arbor, MI.

Kneizys, F. X., E. P. Shettle, W. O. Gallery, J. H. Chetwynd, L. W. Abreu, J. E. A. Selby, S. A. Clough, and R. W. Fenn. 1983. "Atmospheric Transmittance/radiance: Computer Code LOWTRAN 6." Technical Report AFGL–TR–83–0187, Air Force Geophysics Laboratory, Hanscom Air Force Base, MA.

Kneizys, F. X., E. P. Shettle, L. W. Abreu, J. H. Chetwynd, G. P. Anderson, W. O. Gallery, J. E. A. Selby, and S. A. Clough. 1988. "Users Guide to LOWTRAN 7." Technical Report AFGL–TR–88–0177, Air Force Geophysics Laboratory, Hanscom Air Force Base, MA.

Lawrence, R. S. and J. W. Strohbehn. 1970. "A Survey of Clear-air Propagation Effects Relevant to Optical Communications," *Proc. IEEE*, vol. 58, pp. 1523–1545.

Liu, W. T., K. B. Katsaros, and J. A. Businger. 1979. "Bulk Parameterization of Air-sea Exchanges of Heat and Water Vapor Including the Molecular Constraints at the Interface," *Journal of the Atmospheric Sciences*, vol. 36, pp. 1722–1735.

McCartney, E. J. 1976. *Optics of the Atmosphere.* Wiley, New York, NY.

McClatchey, R. A., R. W. Fenn, J. E. A. Selby, F. E. Volz, and J. S. Garing. 1978."Optical Properties of the Atmosphere." In *Handbook of Optics*, pp. 14–13 ff, W. G. Driscoll and W. Vaughn, Eds. McGraw-Hill, New York, NY.

Tatarski, V. I. 1961. *Wave Propagation in a Turbulent Medium*, p. 123, translated by R. A. Silverman. McGraw-Hill, New York, NY.

Wolf, E. 1978. "Coherence and Radiometry" *Journal of the Optical Society of America*, vol. 68, pp. 7–17.

Zeisse, C. R., S. G. Gathman, A. E. Barrios, W. K. Moision, K. L. Davidson, P. A. Frederickson, and B. D. Nener. 1988. "Low Altitude Infrared Transmission." In *Proceedings of the 1997 Battlespace Atmospherics Conference*, Technical Document 2989, pp. 589–599, K. D. Anderson and J. H. Richter, Eds. SSC San Diego, CA.

APPENDIX: CONNECTING SCINTILLATION THEORY TO EXPERIMENT

This appendix establishes a connection between theoretical expressions for the variance of the log-amplitude (and the variance of the log-intensity) and the experimentally measured voltage time series.

We denote the mean of a random variable, x, by μ_x, its variance about the mean by σ_x^2, and its normalized variance about its mean by s_x^2, that is,

$$\begin{aligned} \mu_x &= \langle x \rangle \equiv \int x f(x) dx \\ \sigma_x^2 &= \left\langle \left(x - \langle x \rangle\right)^2 \right\rangle \\ s_x^2 &= \frac{\left\langle \left(x - \langle x \rangle\right)^2 \right\rangle}{\langle x \rangle^2} = \frac{\sigma_x^{\,2}}{\mu_x^2}, \end{aligned} \tag{A1}$$

where $f(x)dx$ is the probability that the random quantity will have a value between x and $x + dx$.

Following Tatarski (1961), we denote a complex optical field amplitude, such as E or H, by the letter, u, and introduce the subscript, o, to indicate a quantity in the absence of turbulence. The complex field amplitude in the presence of turbulence will be

$$u = Ae^{iS} \tag{A2}$$

where S is the turbulent phase, A is the turbulent amplitude, and the complex field amplitude in the absence of turbulence will be

$$u_o = A_o e^{iS_o}. \tag{A3}$$

Furthermore, Tatarski (1961) defines the log-amplitude, χ, by

$$A \equiv A_o e^{\chi}. \tag{A4}$$

The detector produces a voltage linearly proportional to the optical power it receives. In the literature on scintillation, the word "intensity" refers to the square of the modulus of the field amplitude, which is proportional to the Poynting vector, the power per unit area flowing in the field. Since the receiver usually has a fixed area, the detector voltage will be proportional to the complex field amplitude squared. To summarize,

$$V \propto P \propto I \equiv u^* u = A^2 = A_o^2 e^{2\chi} \tag{A5}$$

when there is turbulence, and

$$V_o \propto P_o \propto I_o \equiv u_o^* u_o = A_o^2 \tag{A6}$$

when there is no turbulence. We have no way of measuring V_o since there is always a little turbulence present in the atmosphere and we never can be sure of obtaining absolutely quiet conditions. However, we do know that

$$\frac{V}{V_o} = \frac{I}{I_o} = e^{2\chi} \tag{A7}$$

so that

$$\begin{aligned} \ln I &= \ln I_o + 2\chi \\ \langle \ln I \rangle &= \langle \ln I_o \rangle + 2\langle \chi \rangle = \ln I_o + 2\langle \chi \rangle \\ \ln I - \langle \ln I \rangle &= 2(\chi - \langle \chi \rangle) \\ (\ln I - \langle \ln I \rangle)^2 &= 4(\chi - \langle \chi \rangle)^2 \end{aligned} \tag{A8}$$

or

$$\sigma^2_{\ln V} = \sigma^2_{\ln I} = 4\sigma^2_\chi, \tag{A9}$$

regardless of the value of V_o or I_o.

Experimentally, scintillation has been shown to obey a lognormal distribution, and from now on we will always assume that is the case with experimental data. At this point, we will also abandon the distinction between voltage and intensity since the (generally unknown) proportionality constant between these two quantities will drop out of our analysis. The moments of a log normal distribution (Evans, Hastings, and Peacock, 1993) obey:

$$\langle I^n \rangle \equiv \int_0^\infty I^n f(I) dI = m^n \exp(n^2\sigma^2/2), \tag{A10}$$

where m is the median and σ is called the shape parameter. The square of the shape parameter is identical to the variance of the log-intensity:

$$\sigma^2_{\ln I} \equiv \langle (\ln I - \langle \ln I \rangle)^2 \rangle = \sigma^2. \tag{A11}$$

Applying equation (A10) to the first and second moments of the experimental time series, we have

$$\begin{aligned} \langle I \rangle &= m\exp(\sigma^2/2) \\ \langle I^2 \rangle &= m^2 \exp(2\sigma^2) \\ 1 + s_I^2 &= \frac{\langle I^2 \rangle}{\langle I \rangle^2} = \exp(\sigma^2) = \exp(4\sigma_\chi^2) \end{aligned} \tag{A12}$$

or

$$\ln\left(1+s_V^2\right)=\ln\left(1+s_I^2\right)=\sigma_{\ln I}^2=4\sigma_\chi^2, \tag{A13}$$

which are the relationships we originally sought to establish. Equation (A13) holds for linear detection of scintillation distributed according to a lognormal law.

Table 1. Source and detector properties and 7-km free-space signals in the field. All electrical values are at the detector. Net radiance is the difference in radiance between the black body cavity and the chopper blade. Throughput was not measured but was arbitrarily chosen to provide best agreement with the measured laboratory voltages. Detector noise and the A/D level are given as a per cent of the 7-km free-space signal. "Tau" is the transmission mode and "Chi" is the scintillation mode.

	Longwave Band			Midwave Band		
Parameter	Value		Units	Value		Units
Temperature	1200		K	1200		K
Net Radiance	623.4		$W\ m^{-2}\ sr^{-1}$	3748		$W\ m^{-2}\ sr^{-1}$
Throughput	35		%	45		%
Bias	7		mA	None		---
Responsivity	2740		$V\ W^{-1}$	2.9		$A\ W^{-1}$
Noise	14.3		$nV_{rms}\ Hz^{-1/2}$	3.5		$pA_{rms}\ Hz^{-1/2}$
IR Background	4.4		$nV_{rms}\ Hz^{-1/2}$	1.1		$pA_{rms}\ Hz^{-1/2}$
Free Space (f s)	3.9		μV_{rms}	28.3		nA_{rms}
Mode	Tau	Chi	----	Tau	Chi	----
Bandwidth	0.026	78	Hz	0.026	78	Hz
Detector Noise	0.06	3.3	% f s	0.002	0.1	% f s
1 A/D Level	0.06	0.13	% f s	0.09	0.09	% f s

Table 2. Typical values used during calibration and field operation of the transmissometer. The radiance values are broad band net values; that is, they are differences between the broad band cavity and blade radiance. The field signals are the nominal free-space (100% transmission) values in the detector for a range of 7 km.

Quantity	Symbol	Lab	Field	Units
Blade factor	F	0.450	0.395	----
Source temperature	T	500	1200	K
Net longwave radiance	B	79.40	623.4	W m^{-2} sr^{-1}
Net midwave radiance	B	44.00	3748	W m^{-2} sr^{-1}
Source diameter	D	0.311	6.35	mm
Transmitter focal length	f	1.22	1.22	m
Transmitter diameter	D_{Tx}	20	20	cm
Receiver diameter	D_{Rx}	20	20	cm
Longwave signal	V_{fs}	40	4	μV_{rms}
Midwave signal	V_{fs}	30	30	nA_{rms}

Table 3. Estimates of per cent uncertainty due to measurement imprecision, component non-uniformity, and operational instability.

Quantity	Symbol	Longwave	Midwave
Radiance calculation	B	0.5	0.3
Transmitter area	A_{Tx}	0.26	0.26
Receiver area	A_{Rx}	0.26	0.26
Blackbody area	A_o	2	2
Transmissometer area	A	5	5
Transmitter focal length	f	0.08	0.08
Range	L	0.14	0.14
Throughput inhomogeneity	ρ	1.6	2.4
LN_2 level drift		1.5	0.0
Lock-in phase drift		1.52	1.52
Optical reflectivity drift	ρ	3	3
Responsivity drift (per day)	$\Re$	2	1
Room temperature drift		0.5	0.0
Total Error (Root-Sum-Square)		7.1	6.9
Total Error (Adopted)		10	10

REPORT DOCUMENTATION PAGE

Form Approved
OMB No. 0704-0188

1. AGENCY USE ONLY *(Leave blank)*	2. REPORT DATE	3. REPORT TYPE AND DATES COVERED
	June 1999	Final

4. TITLE AND SUBTITLE

MEASUREMENT OF LOW-ALTITUDE INFRARED TRANSMISSION

5. FUNDING NUMBERS

PE: 0602435N
AN: DN302215
WU: MPB2

6. AUTHOR(S)

C. R. Zeisse
SSC San Diego

B. D. Nener
University of Australia

R. V. Dewees
NAVAIRWARCEN, China Lake

7. PERFORMING ORGANIZATION NAME(S) AND ADDRESS(ES)

SSC San Diego
San Diego, CA 92152–5001

8. PERFORMING ORGANIZATION REPORT NUMBER

TR 1797

9. SPONSORING/MONITORING AGENCY NAME(S) AND ADDRESS(ES)

Office of Naval Research (ONR 322)
800 North Quincy Street
Arlington, VA 22217-5660

10. SPONSORING/MONITORING AGENCY REPORT NUMBER

11. SUPPLEMENTARY NOTES

12a. DISTRIBUTION/AVAILABILITY STATEMENT

Approved for public release; distribution is unlimited.

12b. DISTRIBUTION CODE

13. ABSTRACT *(Maximum 200 words)*

Infrared propagation at low altitudes is determined by extinction caused by molecules, aerosol particles, and ray bending by refraction, three effects that control the mean value of the signal (the transmission). Interference induces fluctuations of the signal (scintillation) about that mean value. This report discusses the design, calibration, and limitations of a field instrument for measuring transmission and scintillation inside the midwave and longwave infrared atmospheric passbands. The instrument, which is accurate to $\pm 10\%$, has been used to investigate aerosol, refractive, and scintillation phenomena in the marine boundary layer.

14. SUBJECT TERMS

Mission Area: Command, Control, and Communications
transmission atmosphere infrared
molecules aerosols refraction
scintillation

15. NUMBER OF PAGES

48

16. PRICE CODE

17. SECURITY CLASSIFICATION OF REPORT	18. SECURITY CLASSIFICATION OF THIS PAGE	19. SECURITY CLASSIFICATION OF ABSTRACT	20. LIMITATION OF ABSTRACT
UNCLASSIFIED	UNCLASSIFIED	UNCLASSIFIED	SAME AS REPORT

21a. NAME OF RESPONSIBLE INDIVIDUAL	21b. TELEPHONE *(include Area Code)*	21c. OFFICE SYMBOL
C. R. Zeisse	(619) 553–3602 e-mail: zeisse@spawar.navy.mil	Code D883

INITIAL DISTRIBUTION

D0012	Patent Counsel	(1)
D0271	Archive/Stock	(6)
D0274	Library	(2)
D027	M. E. Cathcart	(1)
D0271	D. Richter	(1)
D743	C. S. Bendall	(1)
D754	R. M. Carlson	(1)
D88	R. A. Paulus	(1)
D883	S. M. Hammel	(2)
D883	D. R. Jensen	(1)
D883	K. M. Littfin	(1)
D883	C. P. McGrath	(1)
D883	W. K. Moision	(2)
D883	W. L. Patterson	(1)
D883	C. R. Zeisse	(80)

Defense Technical Information Center
Fort Belvoir, VA 22060–6218 (4)

SSC San Diego Liaison Office
Arlington, VA 22202–4804

Center for Naval Analyses
Alexandria, VA 22302–0268

Navy Acquisition, Research and Development
Information Center (NARDIC)
Arlington, VA 22244–5114

GIDEP Operations Center
Corona, CA 91718–8000

Office of Naval Research
Arlington, VA 22217–5660 (4)

Naval Air Warfare Center Weapons Division
China Lake, CA 95333–6001 (5)

Naval Postgraduate School
Monterey, CA 93943–5114 (2)

University of Western Australia
Nedlands, Perth
Western Australia 60090 (20)

TNO Physics and Electronics Laboratory
The Hague, Netherlands (7)

Defence Research Establishment Valcartier
Val–Belair, Quebec, G3J 1X5
Canada (2)

University of Sunderland
Sunderland SR2 7BM
United Kingdom

DERA Portsdown West (MOD)
Fareham, Portsmouth
United Kingdom P017 6AD